Inorganic Chemistry

pubs.acs.org/IC

Article

Temperature-Dependent Products in Gallium Flux Reactions of Cerium and Transition Metals

Md. Sahab Uddin, Amirhossein Zareihassangheshlaghi, and Susan E. Latturner*

Cite This: https://doi.org/10.1021/acs.inorgchem.4c00797

Read Online

ACCESS | Metrics & More | Article Recommendations | Supporting Information

ABSTRACT: Reactions of cerium and transition metals in excess molten gallium were carried out, exploring the formation of different cerium intermetallics as the flux reaction is cooled. Ce/*T*/Ga reactions with *T* = Ni, Cu, Pd, Ag, and Zn produce a high-temperature product, which converts into a low-temperature product in the flux. The phases present in the flux mixture were determined by quenching identical reactions at 750 and 300 °C and identifying the isolated products using elemental analysis and X-ray diffraction. The compounds $CeGa_2$, $CeCu_{0.37}Ga_{3.63}$, $CePd_{0.32}Ga_{3.68}$, $Ce_5Ag_{1.76}Ga_{17.29}$, and $Ce_5Zn_{1.37}Ga_{17.73}$ were isolated by quenching at 750 °C. Upon cooling to 300 °C, the corresponding reactions instead yielded $CeGa_6$, Ce_2CuGa_{12}, Ce_2PdGa_{12}, $Ce_2Ag_{0.7}Ga_{9.1}$, and $CeZn_xGa_{7-x}$. All of these structures contain cerium in the $ThCr_2Si_2$-related layers. Large crystals of high-temperature products $CeCu_{0.37}Ga_{3.63}$, $CePd_{0.32}Ga_{3.68}$, $Ce_5Ag_{1.76}Ga_{17.29}$, and $Ce_5Zn_{1.37}Ga_{17.73}$ were used for magnetic susceptibility measurements. All of these materials show highly anisotropic ferromagnetic ordering of Ce^{3+} moments below 8 K, which is in contrast to the antiferromagnetism seen for the compounds that were isolated at 300 °C.

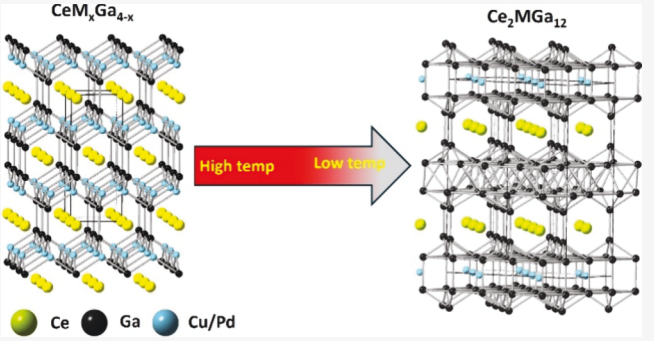

INTRODUCTION

Rare-earth intermetallic compounds exhibit a variety of interesting properties, such as superconductivity ($CeCoIn_5$),[1] thermoelectric behavior ($Yb_{14}MnSb_{11}$),[2] strong ferromagnetism ($Nd_2Fe_{14}B$),[3] and hydrogen storage ($LaNi_5H_6$).[4] Metal flux synthesis has proven to be a useful method to grow rare-earth-containing intermetallics.[5] An excess of low melting metal, or a combination of metals, is used in flux synthesis to act as a solvent for the other species involved in the reaction. This creates a homogeneous solution from which intermetallic compounds can precipitate as the solution is cooled. Several of the limitations of conventional solid-state synthesis, including diffusion barriers and the ensuing lengthy reaction times, repetitive heating cycles, and high temperatures, are mitigated by the use of molten flux. The faster reactions and lower heating temperatures compared to conventional solid-state reactions allow for the formation of kinetic products rather than the thermodynamic phases favored by high temperatures. Moreover, as flux synthesis is a solution-based technique, slow cooling of the melt can result in the growth of sizable crystals.[6] Gallium is of particular interest as a flux due to its low melting point and high boiling point, which enable a broad temperature range for reactions. Ho_2CoGa_8,[7] $CePd_{3+x}Ga_{8-x}$,[8] $Ba_8Ga_{16}Ge_{30}$,[9] $EuGa_2As_2$,[10] and Ce_2NiGa_{12}[11] are intermetallic compounds that can be produced from gallium flux.

The metal flux synthesis method has drawbacks, one of which is the production of many competing phases without knowledge of the reaction mechanism (and consequently limited ability to predict and control reaction outcome). Flux reactions are frequently conducted in sealed ampules at high temperatures inside furnaces, which makes it particularly challenging to detect intermediate phases. Several intermediate phases and end products can emerge when the reaction parameters (reactant ratio, heating rate, maximum temperature, cooling rate, and quench temperature) are changed. In situ diffraction studies, which involve performing a flux reaction in a heated sample holder in a diffractometer to permit the observation of phase transformation events as the temperature is altered, can detect and identify products.[12] This typically requires high-power X-ray sources or neutron beams to penetrate the sample holder and flux. A recent example is the study of the interaction between cerium and nickel in gallium flux using in situ neutron diffraction; results showed that a high-temperature phase ($ThCr_2Si_2$-type $CeNi_{0.74}Ga_{3.26}$) was formed above 800 °C before converting to a low-temperature product (Ce_2NiGa_{12}) below 600 °C.[11]

Received: February 26, 2024
Revised: May 30, 2024
Accepted: June 3, 2024

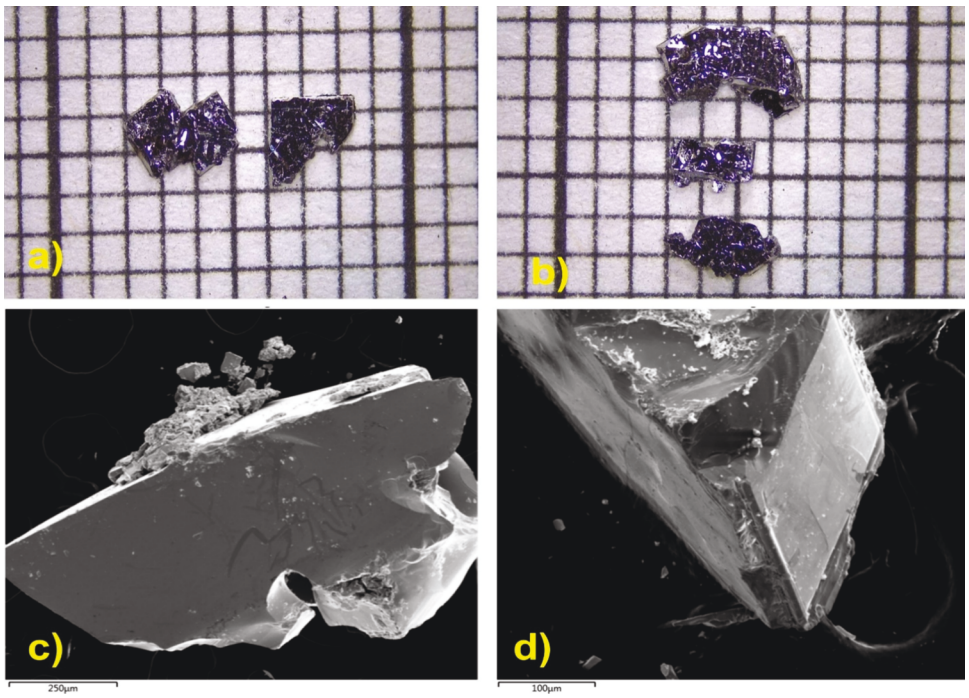

Figure 1. Crystals of Ce/T/Ga products grown from gallium flux at 750 °C. Optical microscopy images on 1 mm grid paper of clusters of plate-like crystals of (a) $CeCu_{0.37}Ga_{3.63}$ and (b) $CePd_{0.32}Ga_{3.68}$. (c/d) Scanning electron microscopy image of $CePd_{0.32}Ga_{3.68}$ showing the top and cross-sectional view of the crystal.

Table 1. Crystallographic Data and Collection Parameters for Four High-Temperature Products of Reactions of Cerium with Transition Metals in a Gallium Flux

formula	$Ce_5Ag_{1.76}Ga_{17.29}$	$Ce_5Zn_{1.37}Ga_{17.73}$	$CeCu_{0.37}Ga_{3.63}$	$CePd_{0.32}Ga_{3.68}$
formula weight (g/mol)	2095.56	2026.29	416.71	430.92
crystal system	tetragonal	tetragonal	tetragonal	tetragonal
space group	$I4/m$	$I4/m$	$I4/mmm$	$I4/mmm$
a (Å)	9.7404(2)	9.7411(3)	4.3105(1)	4.3422(1)
c (Å)	10.1501(6)	10.1167(4)	10.4828(3)	10.5294(6)
Z	2	2	2	2
volume (Å^3)	963.01(7)	959.96(7)	194.775(11)	198.529(15)
density, calc (g/cm^3)	7.227	7.010	7.105	7.209
index ranges	$-15 \le h \le 14$	$-16 \le h \le 14$	$-7 \le h \le 7$	$-7 \le h \le 6$
	$-14 \le k \le 14$	$-16 \le k \le 14$	$-7 \le k \le 7$	$-6 \le k \le 7$
	$-16 \le l \le 16$	$-16 \le l \le 17$	$-17 \le l \le 17$	$-17 \le l \le 16$
reflections collected	5067	6588	4457	2067
temperature (K)	290	297	300	298
radiation	Mo Kα	Mo Kα	Mo Kα	Mo Kα
unique data/parameters	1079/32	1317/33	188/9	160/10
μ (mm^{-1})	36.959	37.615	37.967	37.045
R_1/wR_2 ($I > 2\sigma(I)$)	0.0297/0.0835	0.0471/0.1261	0.0201/0.0511	0.0298/0.0635
R_1/wR_2 (all data)	0.0377/0.0871	0.0414/0.1224	0.0201/0.0511	0.0320/0.0646
highest peak/hole (e−/Å^3)	3.345/−2.482	7.634/−4.271	1.679/−2.087	1.583/−3.366
CCDC deposition	2324748	2324749	2324750	2324751

In the absence of beamtime at a synchrotron or neutron source, flux syntheses can be monitored by quenching the reaction at different temperatures. In this work, gallium flux reactions of cerium with other elements were carried out and quenched at high (750 °C) and low (300 °C) temperatures to investigate the compounds present at these temperatures. Binary (Ce/Ga) and ternary (Ce/T/Ga, where T = Cu, Pd, Ag, or Zn) systems were investigated. All the reactions yielded high-temperature compounds present at 750 °C that were different from those isolated from identical reactions cooled to 300 °C. Comparison of structures and compositions of the high-temperature and low-temperature products allow for better understanding of the mechanism of phase transitions that occur in the flux as it cools.

EXPERIMENTAL PROCEDURE

Synthesis. Reactions were prepared using the following elements: Ce chunks (Alfa-Aesar, rare earth metal basis, 99%), Cu powder (Alfa-Aesar, metal basis, 99.8%), Pd powder (Alfa-Aesar, metal basis, 99.8%), Ag powder (Alfa-Aesar, metal basis, 99.99%), Zn powder

https://doi.org/10.1021/acs.inorgchem.4c00797
Inorg. Chem. XXXX, XXX, XXX−XXX

Table 2. Reactants and Observed Products for Ce/*T*/Ga Flux Reactions Centrifuged at Different Temperatures[a]

reactants	reactant ratio (mmol)	quench temp. (°C)	products	elemental analysis (Ce: T: Ga)[b]	space group, structure type	unit cell parameters (Å)
Ce/Ga	1:10	750	$CeGa_2$	25.4:74.6	*P6/mmm*	a = 4.3282(4)
					AlB_2	c = 4.3456(4)
Ce/Ga	1:10	300	$CeGa_6$	14.4:85.6	*P4/nbm*	a = 6.0459(2)
					$PuGa_6$	c = 7.6785(3)
Ce/Cu/Ga	1:0.5:10	750	$CeCu_{0.37}Ga_{3.63}$	21.2:7.6:71.3	*I4/mmm*	a = 4.3105(1)
					$ThCr_2Si_2$	c = 10.4828(3)
Ce/Cu/Ga	1:0.5:10	300	Ce_2CuGa_{12}	13.3:7.9:78.8	*P4/nbm*	a = 6.0998(3)
					Ce_2CuGa_{12}	c = 15.361(1)
Ce/Pd/Ga	1:0.5:10	750	$CePd_{0.32}Ga_{3.68}$	20.6: 8.5:70.9	*I4/mmm*	a = 4.3422(1)
					$ThCr_2Si_2$	c = 10.5294(6)
Ce/Pd/Ga	1:0.5:10	300	Ce_2PdGa_{12}	13.5: 7.0:79.5	*P4/nbm*	a = 6.1027(3)
					Ce_2CuGa_{12}	c = 15.606(2)
Ce/Ag/Ga	1:0.5:10	750	$Ce_5Ag_{1.76}Ga_{17.29}$	18.2:8.9:72.9	*I4/m*	a = 9.7404(2)
					Rb_5Hg_{19}	c = 10.1501(6)
Ce/Ag/Ga	1:0.5:10	300	$CeGa_6$	13.6:86.4	*P4/nbm*	a = 6.0502(3)
					$PuGa_6$	c = 7.6812(4)
Ce/Zn/Ga	1:0.5:10	750	$Ce_5Zn_{1.37}Ga_{17.73}$	22.7:5.6:71.7	*I4/m*	a = 9.7411(3)
					Rb_5Hg_{19}	c = 10.1167(4)
Ce/Zn/Ga	1:0.5:10	300	$CeZn_{0.4}Ga_{6.6}$	13.1:4.9:82	*P4/mmm*	a = 4.3005(2)
					$CePdGa_6$	c = 7.6913(4)

[a]Unit cell parameters for products were determined from SC-XRD; elemental analysis data were from SEM-EDS. [b]Atomic percentages of SEM-EDS averaged from 3 to 4 crystals; values are ±1%.

(Alfa-Aesar, metal basis, 99.9%), and Ga chips (Alfa-Aesar, 99.9%). Reactants were used as received, with the oil coating of the cerium chips removed by quickly rinsing in hexanes before weighing and placing in the reaction ampule. Reactants were weighed out and then combined in a Ce/T/Ga 1:0.5:10 mmol ratio in a quartz ampule (7 mm ID, 9 mm OD). For instance, the Ce/Cu/Ga reaction was prepared using 0.140 g:0.0317 g:0.697 g masses of the respective elements. Fiberfrax wool was placed above the reactants to act as a filter during centrifugation. This silica ampule was then sealed under a vacuum at 100 mTorr. For each system, two identical reactions were prepared that were subjected to different heating profiles. To isolate high-temperature products, the reactions were heated to 1000 °C, held for 24 h, then cooled to 750 °C in 72 h, removed from the furnace at that temperature, and centrifuged to remove the excess flux and thereby stop the reaction. To isolate low-temperature products, the heating profile was identical except the reactions were cooled to 300 °C in 72 h and centrifuged at that temperature. All products (of both high- and low-temperature reactions) were air-stable silver/gray powders and crystals (see Figure 1).

Powder X-ray Diffraction. Samples isolated from the flux reactions by centrifugation were ground to a powder in an alumina mortar and pestle. The powders were placed on a zero-background sample holder (oriented single crystal of silicon), and diffraction data were acquired using a Rigaku SmartLab diffractometer with a Cu−Kα radiation source. Data were collected in the 2θ range 10°−80°. The resulting patterns were analyzed with the search-match feature to determine the Ce/*T*/Ga phases present in the sample.

Single-Crystal X-ray Diffraction. Most of the Ce/*T*/Ga flux reactions yielded crystals suitable for SC-XRD. Low-temperature compounds with structures already reported in the literature were not analyzed, but full data collections were carried out on the crystals of $CeCu_{0.37}Ga_{3.63}$, $CePd_{0.32}Ga_{3.68}$, $Ce_5Zn_{1.37}Ga_{17.73}$, and $Ce_5Ag_{1.76}Ga_{17.29}$ which were isolated at 750 °C. Using an optical microscope, pieces were cut from larger crystals and mounted on cryoloops using parabar oil. Single-crystal X-ray diffraction data were collected at 294 K using a Rigaku XtaLAB Synergy-S diffractometer equipped with a HyPix-6000HE Hybrid Photon Counting (HPC) detector and a dual Mo−Kα and Cu−Kα microfocus sealed X-ray source. Data collection and initial indexing and processing of data were carried out using the CrysAlis Pro software;[13] refinements of structures were performed with the SHELXTL package using the SHELXLe interface.[14] For $Ce_5Zn_{1.37}Ga_{17.73}$, distinguishing the Zn and Ga sites relied on elemental analysis, with the Zn/Ga mixed site constrained to match the ratio indicated by SEM data. Crystallographic information for the four analyzed compounds is listed in Table 1; CIF files have been deposited with the Cambridge Crystallographic Data Centre (deposition numbers listed in Table).

Elemental Analysis. An FEI Nova 400 Nano SEM with energy-dispersive spectroscopy (EDS) capability was used to conduct SEM-EDS analyses of the products. Double-sided carbon tape was used to mount the product crystal samples onto aluminum pucks for analysis. Measurements were conducted using a 20 kV acceleration voltage on cleaved samples or on homogeneous surfaces. Despite attempts to scrape off any gallium residue from the crystals, the surface of many of the crystals had droplets of the gallium flux residue in some places. Therefore, the best data acquisition locations were found by initially mapping the scanned surface of the samples, which shows the distinct difference between the crystal surface and the areas of the flux residue on the crystals. Observed elemental ratios are listed in Table 2; corresponding SEM-EDS spectra are found in Supporting Information (Figure S1).

Magnetic Susceptibility Measurements. Magnetic susceptibility data were collected on single crystals using a Quantum Design MPMS SQUID magnetometer to determine potential magnetic ordering and to characterize cerium's valence state. The crystals of $CeCu_{0.37}Ga_{3.63}$, $CePd_{0.32}Ga_{3.68}$, $Ce_5Zn_{1.37}Ga_{17.73}$, and $Ce_5Ag_{1.76}Ga_{17.29}$ which formed like a plate were positioned with their crystallographic ab axis parallel to the applied field by aligning it on a Kapton tape. Following that, this tape was put into a straw and fastened to the specimen rod of a Quantum Design MPMS SQUID instrument. Data on magnetic susceptibility, expressed as χ = M/H, was acquired from 1.8 to 300 K with a 500 Oe applied magnetic field. Zero-field-cooled (ZFC) and field-cooled (FC) data were also collected with the ab axis of the crystals parallel and perpendicular to the magnetic field from 1.8 to 300 K with a 500 Oe applied magnetic field. Measurements of magnetization were made at 2 K as the field scaled from 7.0 to −7.0 T for both orientations of the crystallographic *ab*-plane. The data was collected afterward with the crystal repositioned so that the *ab*-plane was perpendicular to the applied field. Raw data are found in the

https://doi.org/10.1021/acs.inorgchem.4c00797
Inorg. Chem. XXXX, XXX, XXX−XXX

Supporting Information (Figures S2–S5); fitted data are shown and discussed later in the article.

RESULTS AND DISCUSSION

Previous in situ neutron diffraction studies on the Ce/Ni/Ga system (reaction ratio 1:0.5:10 mmol) indicate that two compounds are formed during the cooling of this reaction. Tetragonal $ThCr_2Si_2$-type $CeNi_{0.74}Ga_{3.26}$ precipitates from the melt as it cools to 800 °C; this is then converted to a low-temperature phase (Ce_2NiGa_{12}) as the reaction cools below 500 °C.[11] Other explorations of reactions in gallium flux have also indicated a change in the products with quenching temperature. Chan et al. isolated α-$Ln$$NiGa_4$ at high temperatures which converted to β-$Ln$$Ni_{1-x}Ga_4$ at lower temperatures (Ln = Tb − Er); they also noted temperature-dependent differences in the Ce/Pd/Ga system (vide infra).[15] These conversions that occur in gallium flux reactions may possibly be linked to the change in local structure and bonding of the molten gallium solvent that occurs around 1000 K (727 °C), which was observed in both high-temperature NMR studies and synchrotron X-ray pair distribution function studies of molten gallium.[16,17] In the absence of in situ neutron diffraction facilities, we have carried out several Ce/T/Ga reactions, quenching them (by removing from the furnace and decanting the excess gallium via centrifugation to stop the reaction) above and below this transition; the products were analyzed using SEM-EDS, PXRD, and SC-XRD and are listed in Table 2. Additional information about product ratios is found in the Supporting Information (Table S1).

Cerium/Gallium Binary System (Ce/Ga). The reaction of 1 mmol of cerium in 10 mmol of gallium produced two observable products. The powder X-ray diffraction patterns of powdered samples are shown in Figure 2. When the reaction is quenched at 750 °C, the predominant phase is $CeGa_2$ with the hexagonal AlB_2 structure type; these crystals form as silver rods with a hexagonal cross-section. When the reaction is quenched at 300 °C, the predominant phase is $CeGa_6$ with the tetragonal $PuGa_6$ structure type; these crystals form as silver plates. This indicates conversion from $CeGa_2$ to $CeGa_6$ as the temperature drops. Some traces of $CeGa_6$ are seen in the PXRD data of the high-temperature product, likely forming as the reaction ampule is removed from the furnace and quickly transferred into the centrifuge (the temperature drop during this process may induce the formation of some of the lower temperature phase).

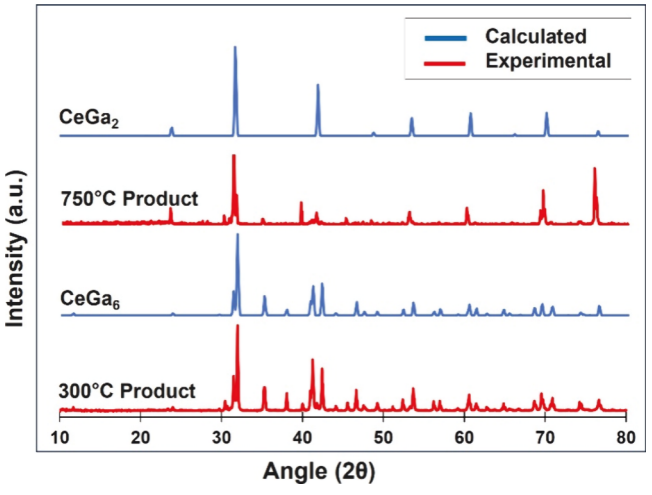

Figure 2. PXRD data for products of reactions of cerium in gallium flux (Ce/Ga 1:10 mmol ratio), centrifuged at 750 or 300 °C.

Cerium/Copper/Gallium System (Ce/Cu/Ga). The PXRD data for products isolated at different temperatures from the reactions of cerium and copper in excess gallium are shown in Figure 3. The reaction quenched at a high temperature (750 °C) produces tetragonal $ThCr_2Si_2$-type $CeCu_{0.37}Ga_{3.63}$; the crystals have a silver plate-like habit, which leads to evidence of preferred orientation in the PXRD data. This compound reacts upon cooling in the flux to form silvery ash color crystals of Ce_2CuGa_{12} isolated at 300 °C. These product structures and their formation in gallium flux are similar to what was observed in the previously reported Ce/Ni/Ga reaction system ($CeNi_{0.74}Ga_{3.26}$ precipitating at 850 °C and converting to Ce_2NiGa_{12} below 500 °C).

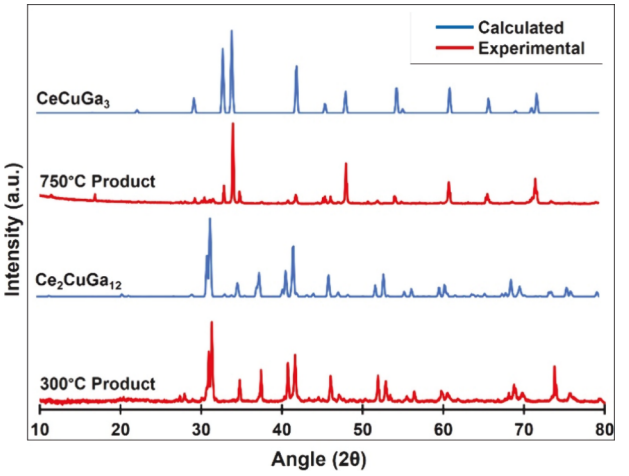

Figure 3. PXRD data for products of Ce/Cu/Ga reactions (1:0.5:10 mmol ratio), centrifuged at 750 or 300 °C.

Cerium/Palladium/Gallium System (Ce/Pd/Ga). The Ce/Pd/Ga system behaves similarly to the Ce/Ni/Ga and Ce/Cu/Ga systems. The PXRD data shown in Figure 4 indicate that tetragonal $ThCr_2Si_2$-type $CePd_{0.32}Ga_{3.68}$ is present in the flux at high temperatures (trace amounts of $CePdGa_6$ are also

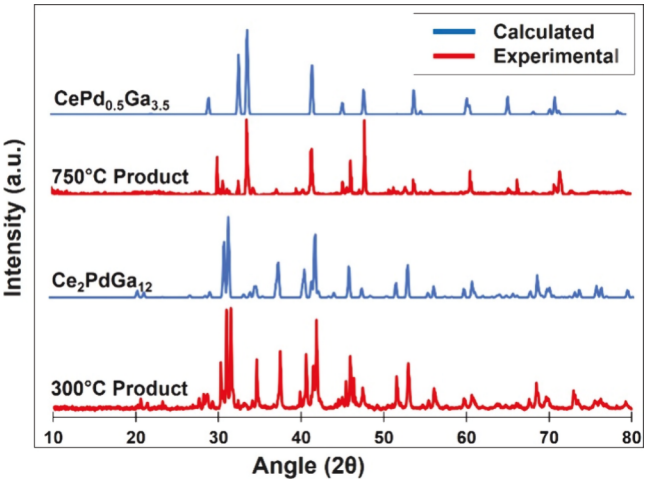

Figure 4. PXRD data for products of Ce/Pd/Ga reactions in a 1:0.5:10 mmol ratio, centrifuged at 750 or 300 °C.

https://doi.org/10.1021/acs.inorgchem.4c00797
Inorg. Chem. XXXX, XXX, XXX−XXX

indicated). The crystals of $CePd_{0.32}Ga_{3.68}$ isolated by centrifuging at 750 °C have a silver plate-like habit. This high-temperature phase then converts to Ce_2CuGa_{12}-type Ce_2PdGa_{12} as the flux cools. Trace amounts of $CeGa_6$ are also seen in the products isolated at 300 °C. Reactions of cerium and palladium in gallium flux were also explored by Chan et al. at a different reactant ratio (1:1−1.5:20 Ce/Pd/Ga).[18] They noted the effects of both the quench temperature and cooling rate, with $CePdGa_6$, Ce_2PdGa_{10}, and Ce_2PdGa_{12} forming under different conditions. Their quench temperatures were all below 500 °C, which may be the reason why no $ThCr_2Si_2$-type product was isolated in that work.

Cerium/Silver/Gallium System (Ce/Ag/Ga). The PXRD pattern in Figure 5 for the product of the reaction of cerium

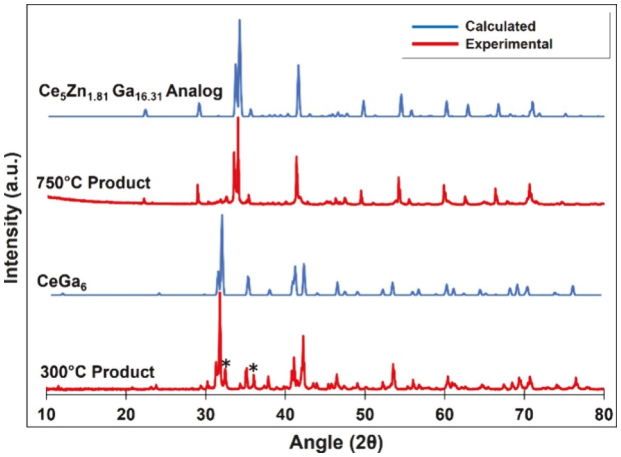

Figure 5. PXRD data for products of Ce/Ag/Ga reactions in a 1:0.5:10 mmol ratio, centrifuged at 750 or 300 °C. Asterisks* denote the diffraction peaks for $Ce_2Ag_{0.7}Ga_{9.1}$ at 300 °C.

and silver in excess gallium quenched at 750 °C matched an existing compound in the database $Ce_5Zn_2Ga_{17}$ with the Rb_5Hg_{19} structure type. This indicates formation of a silver-containing analogue, $Ce_5Ag_xGa_{19-x}$. Upon cooling in the flux, this compound reacts to form predominantly $CeGa_6$ with a small amount of $Ce_2Ag_{0.7}Ga_{9.1}$ byproduct seen in the reaction quenched at 300 °C. Growth of $Ce_2Ag_{0.7}Ga_{9.1}$ from a gallium flux reaction was also reported by Chan et al; their reaction was quenched at 400 °C, so higher-temperature products were not observed.[19]

Cerium/Zinc/Gallium System (Ce/Zn/Ga). The Ce/Zn/Ga system shows similarities to the Ce/Ag/Ga system. PXRD data (Figure 6) shows that the reaction of cerium and zinc in excess gallium quenched at 750 °C yields $Ce_5Zn_{1.37}Ga_{17.73}$ (an analogue of the Rb_5Hg_{19} structure type, as was seen for the Ce/Ag/Ga system) and a small amount of $CeGa_6$ as the byproduct. The crystals of $Ce_5Zn_{1.37}Ga_{17.73}$ separated by centrifugation at 750 °C have a silvery plate habit. Upon cooling in the flux, this compound reacts to form predominantly $CeGa_6$ with a trace amount of $CeZn_{0.4}Ga_{6.6}$ ($CePdGa_6$ structure type) in the reaction quenched at 300 °C.

Single-Crystal X-ray Diffraction Studies. *High-Temperature CeT_xGa_{4-x} Compounds (T = Cu, Pd) with $ThCr_2Si_2$-Type Structure.* Reactions of cerium with T = Cu or Pd in gallium flux quenched at 750 °C yield CeT_xGa_{4-x} products with the $ThCr_2Si_2$ structure type in the tetragonal space group $I4/mmm$. As these reactions cool, these compounds react with gallium flux and are subsequently converted to low-temper-

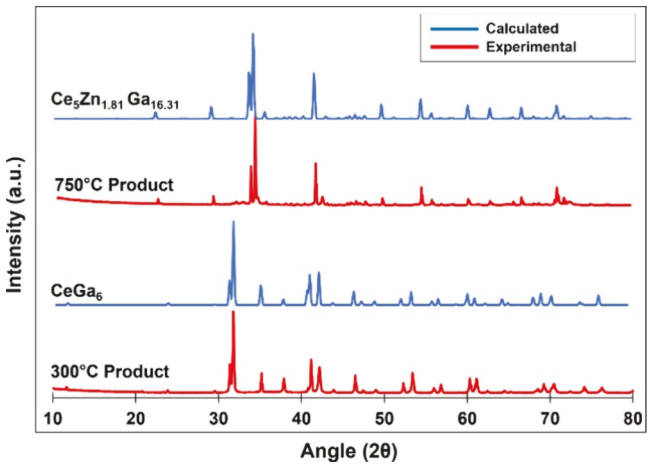

Figure 6. PXRD data for products of Ce/Zn/Ga reactions in a 1:0.5:10 mmol ratio, centrifuged at 750 or 300 °C.

ature Ce_2TGa_{12} products isolated at 300 °C. This is identical to the behavior previously reported for the Ce/Ni/Ga system, in which $CeNi_{0.74}Ga_{3.26}$ precipitated at high temperature and then converted to Ce_2NiGa_{12} below 500 °C.[11] The structure of the CeT_xGa_{4-x} high-temperature phases found here is very similar to those reported by Grin et al., who explored the substitution ranges of various metals into $ThCr_2Si_2$-type gallides using arc-melted stoichiometric mixtures; see Table 3.[20] Incorporation of the third element stabilizes this structure

Table 3. $ThCr_2Si_2$-type CeT_xGa_{4-x} (T = Ni, Cu, or Pd) Phases Formed in Gallium Flux, Compared with Literature Data

compound	a (Å)	c (Å)	M site	reference
$CeNi_{0.7}Ga_{3.3}$	4.3157(8)	10.3093(5)	4e	11
$CeCu_{0.37}Ga_{3.63}$	4.3105(1)	10.4828(3)	4e	This work
$CeCu_{0.4}Ga_{3.6}$	4.313(1)	10.286(3)	4e (assumed)	20
$CePd_{0.32}Ga_{3.68}$	4.3422(1)	10.5294(6)	4e	this work
$CePd_{0.25}Ga_{3.75}$	4.343(1)	10.223(3)	4e	21

type; binary phase $CeGa_4$ is not known. There are two gallium sites (4d and 4e Wyckoff sites) in the structure, as shown in Figure 7. The transition metal can theoretically mix on either of these sites, but it favors the 4e site in all the analogues

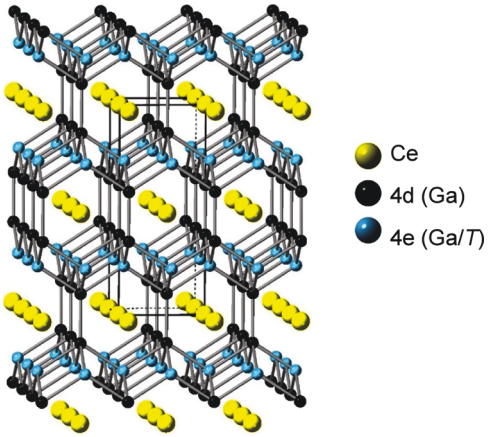

Figure 7. Tetragonal $ThCr_2Si_2$ structure of CeT_xGa_{4-x} compounds (T = Cu or Pd), viewed down the a-axis. T mixes on the 4e site.

https://doi.org/10.1021/acs.inorgchem.4c00797
Inorg. Chem. XXXX, XXX, XXX−XXX

studied so far. The amount of incorporation of Cu and Pd is similar, yielding an overall composition of CeT_xGa_{4-x} with x = 0.3 to 0.4 (for the Cu analogue, the 4d and 4e sites were assigned as Ga, and then their occupancy was allowed to be refined. The occupancy of the 4e site was less than unity and was then constrained to be a mixture of Cu and Ga based on elemental analysis. This results in a composition of $CeCu_{0.37}Ga_{3.63}$). This reflects the 2:1 reactant ratio of Ce to T used in the flux. It is notable that the c-axis unit cell parameters for these flux-grown compounds are significantly longer than those observed by Grin.[21,20] This may be due to a different data collection temperature or slightly different transition metal content.

Low-Temperature Ce_2TGa_{12} Products (T = Cu, Pd). Data from single-crystal X-ray diffraction on crystals isolated from Ce/T/Ga (T = Cu, Pd) reactions centrifuged at 300 °C agreed with the structures of Ce_2CuGa_{12} and Ce_2PdGa_{12} that had previously been published (Figure 8).[11,22] In the in situ neutron diffraction studies of the Ce/Ni/Ga system, the $CeNi_{0.74}Ga_{3.26}$ → Ce_2NiGa_{12} conversion happens as the temperature cools below 550 °C; the conversion temperatures for the Cu and Pd systems may be similar. A comparison of the high-temperature (Figure 7) and low-temperature (Figure 8) structures shows that the cerium coordination environment is maintained, but more gallium is incorporated from the flux. The behavior of the binary (Ce/Ga) system bears some relation to this. Cerium reacts in excess gallium to form $CeGa_2$ (hexagonal AlB_2-type) that is present at 750 °C; this reacts with the gallium flux and converts to tetragonal $CeGa_6$ which is isolated at a low temperature. The $CeGa_6$ structure (Figure 8) contains a layer of gallium very similar to that seen in Ce_2TGa_{12}, which can be viewed as an intergrowth of $ThCr_2Si_2$-type layers with $CeGa_6$-type gallium slabs. This indicates that in all the Ce/T/Ga systems, lowering the temperature induces the incorporation of more gallium from the flux, which forms the gallium slabs present in both structures in Figure 8.

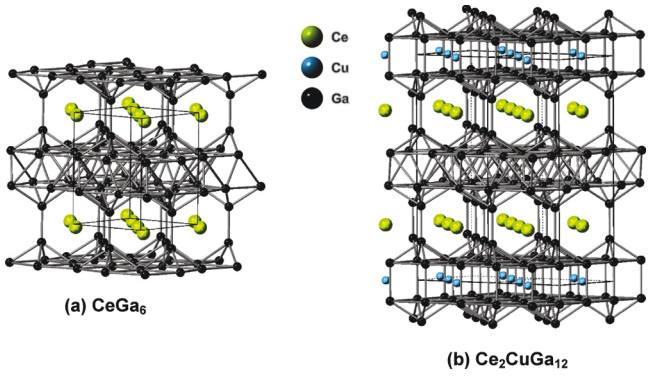

Figure 8. Structures of products isolated at low temperature, both viewed down the [110] direction. (a) $CeGa_6$ ($P4/nbm$, $PuGa_6$ type) from Ce/Ga 1:10 mmol reactions. (b) Ce_2CuGa_{12} ($P4/nbm$) from Ce/Cu/Ga 1:0.5:10 mmol reactions.

Ce/Ag/Ga and Ce/Zn/Ga Systems. The reaction of cerium and T = Ag or Zn in excess gallium yields products with different structures than those seen for T = Ni, Cu, Pd. However, they do show building blocks similar to the $ThCr_2Si_2$ intergrowth structures seen for the Ce/T/Ga (T = Ni, Cu, Pd) systems. The high-temperature phase seen for both the Ce/Ag/Ga and Ce/Zn/Ga systems is $Ce_5T_xGa_{19-x}$, with the Rb_5Hg_{19} structure type in $I4/m$ (see Figure 9). The zinc analogue $Ce_5Zn_2Ga_{17}$ was previously reported by Verbovytskyy et al.[23] The cerium sites are encapsulated by gallium and zinc cages, creating layers that were described by Verbovytskyy as being related to deformed $ThCr_2Si_2$ type slabs. For their zinc analogue, the mixing of Zn on Ga sites was not refined due to their similar X-ray scattering factors; all four Ga sites were assumed to incorporate Ga/Zn at a constant ratio.

The isolation of a silver-containing analogue of this structure from the reaction of cerium and silver in gallium flux enables refinement of the Ga and Ag siting. All of the framework sites were initially assigned as gallium, and the occupancy of each was then allowed to refine. Three of the gallium sites were fully occupied by gallium (2a, 4d, and 16i). The remaining site Ga3 (a different 16i site) had a higher than 100% occupancy and is therefore the preferred site for silver mixing; this is shown as

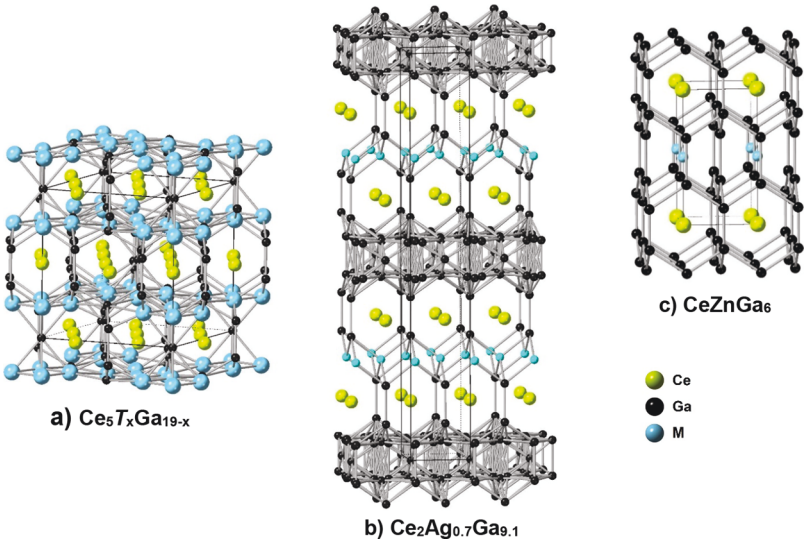

Figure 9. Structures of products observed in the Ce/Ag/Ga and Ce/Zn/Ga reaction systems. (a) High-temperature quenching at 750 °C yield products with the $Ce_5T_xGa_{19-x}$ structure (T = Ag, Zn). At lower temperature, (b) $Ce_2Ag_{0.7}Ga_{9.1}$ is formed in the Ce/Ag/Ga system, and (c) $CeZnGa_6$ is formed in the Ce/Zn/Ga system.

https://doi.org/10.1021/acs.inorgchem.4c00797
Inorg. Chem. XXXX, XXX, XXX−XXX

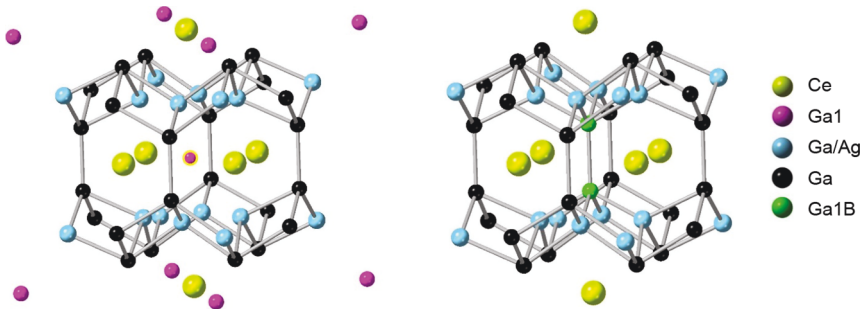

Figure 10. Position of the Ga1 site (magenta) compared to the consistently observed residual electron density peak (Ga1B, green spheres) that forms a dimer in $Ce_5Ag_{1.76}Ga_{17.29}$.

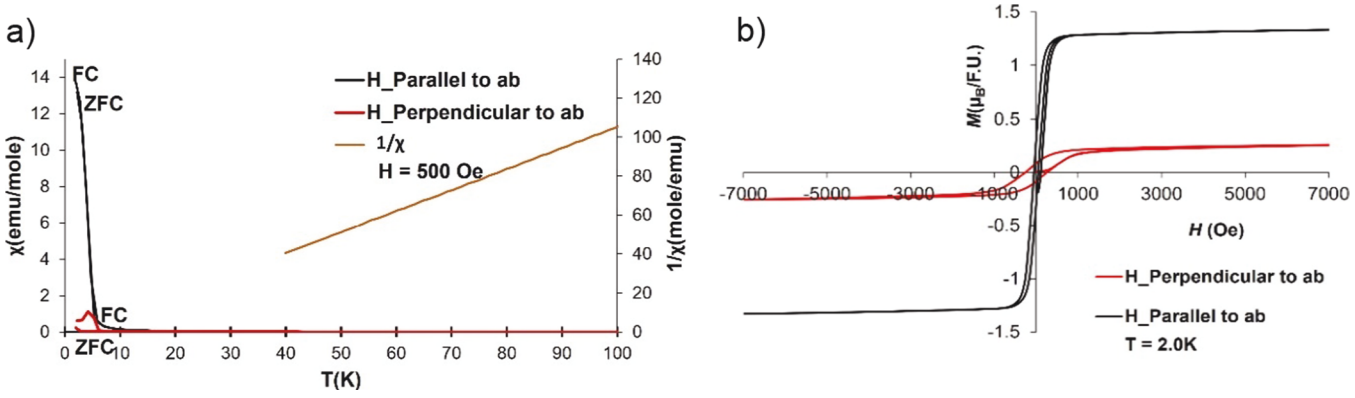

Figure 11. Magnetic susceptibility data for $CePd_{0.32}Ga_{3.68}$. (a) Temperature-dependent magnetic susceptibility (χ) and inverse magnetic susceptibility data; ZFC (zero-field-cooled) and FC (field-cooled) splitting for both parallel (black) and perpendicular (red) orientations of the *ab*-plane to the applied field of H = 500 Oe. (b) Field dependence of magnetization collected at 2 K in both orientations.

blue spheres in Figure 9. However, when the Ga/Ag mixing on this site was allowed to freely refine, it indicated a lower silver content than that shown by elemental analysis. Therefore, the gallium and silver content on this site was constrained to 78.0 and 22.0%, respectively, to match the observed composition. The resulting composition is $Ce_5Ag_{1.76}Ga_{17.29}$.

It is notable that there is a consistent observation of a high residual electron density peak in all data sets for this compound. This electron density peak (on a 4e Wyckoff site) corresponds to a Ga−Ga dimer, which may be replacing the Ga1 atom (2a site) in some unit cells. This dimer (with a Ga−Ga distance of 2.52 Å) is shown in Figure 10. The presence of a Ga−Ga dimer instead of the Ga1 atom brings the structure closer to that of $ThCr_2Si_2$. Putting this "Ga1B" atom into the structure and allowing its position and occupancy to vary freely led to unstable refinements. Therefore, its position along the *c*-axis was fixed, and its occupancy was linked to that of Ga1 (if Ga1 is present, the Ga1B dimer is not). Its thermal parameter was constrained to an isotropic value similar to those of other gallium sites. The refined occupancies indicated that Ga1 is present 95.3% of the time, and the Ga1B dimer is 4.7% occupied. This resulted in a significantly lower *R*-value and elimination of high residual density peaks. The replacement of the Ga1 atom with a dimer of Ga1B atoms results in a slight change in overall composition from that of the Rb_5Hg_{19} parent compound; the resulting formula is $Ce_5Ag_{1.76}Ga_{17.29}$. Atom positions, occupancies, and thermal parameters are listed in Table S2. The distances from surrounding atoms to the Ga1B dimer are somewhat short (2.24 Å), but localized distortions may occur to elongate these bonds.

Quenching the Ce/Ag/Ga reaction at a lower temperature results in conversion to a $Ce_2Ag_{0.7}Ga_{9.1}$ product that incorporates more gallium from the flux within slabs along the *ab*-plane that separates layers of cerium sites surrounded by gallium cages. This disordered Ce_2NiGa_{10}-type structure was previously seen by Chan et al.[19] It is an intergrowth structure of $ThCr_2Si_2$ and fluorite layers, as is the Ce_2NiGa_{12} structure type (Figure 8) that forms at low temperature in the Ce/*T*/Ga (*T* = Ni, Cu, or Pd) systems.

In the Ce/Zn/Ga system, refinement of Zn/Ga mixing from the single-crystal XRD data is not possible due to their near-identical electron counts. However, the crystal structure types are still evident in both PXRD and SC-XRD. Similar to the Ce/Ag/Ga system, reactions quenched at 750 °C yielded an Rb_5Hg_{19}-type compound, $Ce_5Zn_xGa_{19-x}$ (see Figure 9). This is isostructural to the $Ce_5Zn_2Ga_{17}$ initially reported by Verbovytskyy et al. They assumed that all four Ga sites would incorporate Ga/Zn at a constant ratio.[23] However, given the site preference seen in our silver analogue described above (where Ga/Ag mixing is only seen on a 16i site), we postulate that Zn may also exhibit a similar site preference. When the occupancy of all four unique gallium sites was allowed to freely refine, one (16i site) refined with an occupancy higher than the rest. We assume this is where the Ga/Zn mixing occurs and therefore constrained this site as a mixture of the elements at a ratio that results in the observed elemental analysis (17.1% Zn and 82.9% Ga on this 16i site). However, this is based on several assumptions, and additional characterization methods, such as neutron diffraction, would be needed to verify this. Partial occupancies on the other gallium sites were also

https://doi.org/10.1021/acs.inorgchem.4c00797
Inorg. Chem. XXXX, XXX, XXX−XXX

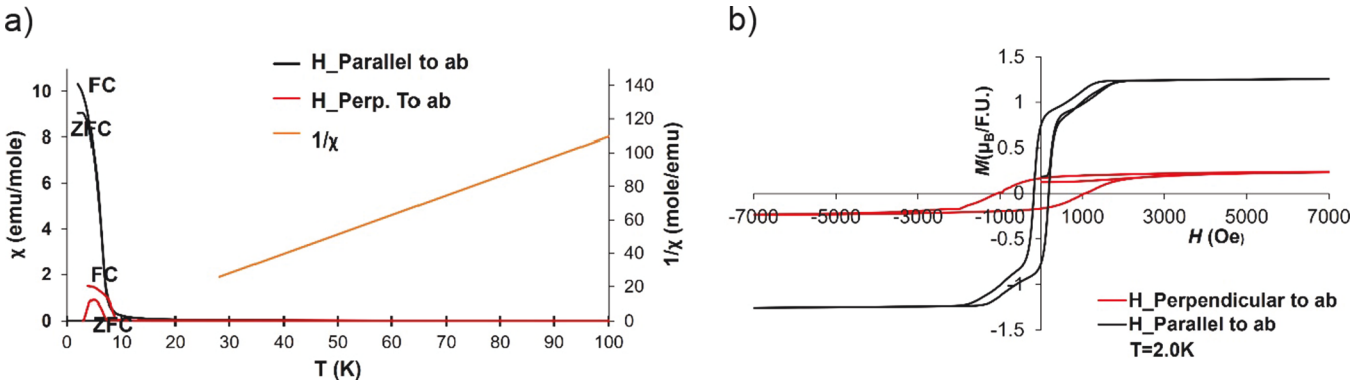

Figure 12. Magnetic susceptibility data for $CeCu_{0.37}Ga_{3.63}$. (a) Temperature-dependent magnetic susceptibility (χ) and inverse magnetic susceptibility ($1/\chi$) data; ZFC (zero-field-cooled) and FC (field-cooled) splitting for both parallel (black) and perpendicular (red) orientations of the *ab*-plane to the applied field of H = 500 Oe. (b) Field dependence of magnetization collected at 2 K in both orientations.

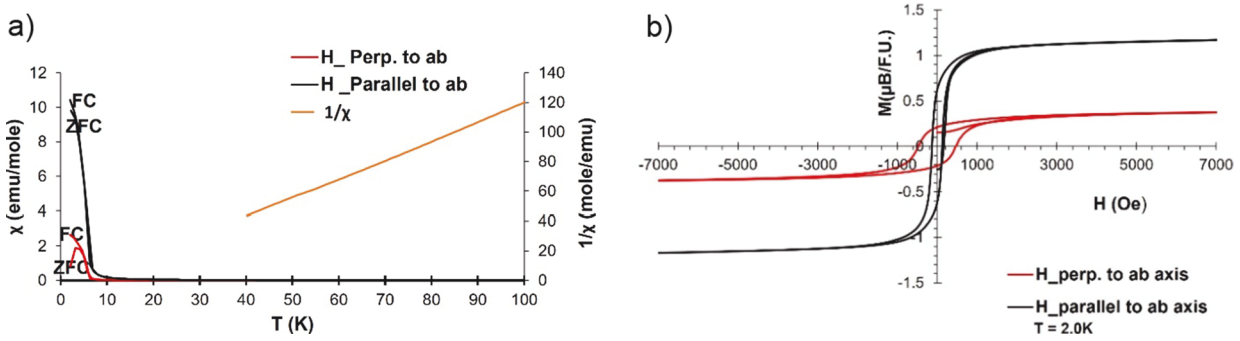

Figure 13. Magnetic susceptibility data for $Ce_5Ag_{1.76}Ga_{17.29}$. (a) Temperature-dependent magnetic susceptibility (χ) and inverse magnetic susceptibility ($1/\chi$) data; ZFC (zero-field-cooled) and FC (field-cooled) splitting for both parallel (black) and perpendicular (red) orientations of the *ab*-plane to the applied field of H = 500 Oe. (b) Field dependence of magnetization collected at 2 K in both orientations.

indicated by Verbovytskyy, but they were not observed in our data.

The same large residual density peak that was consistently observed for the silver analogue is also present for the zinc analogue. This was treated in a similar manner, adding a "Ga1B" site that forms a partially occupied dimer. The position and isotropic thermal parameter of this atom were fixed, and the occupancy was constrained to refine along with the Ga1 site. The results indicate the Ga1 atom (2a site) is present 89.3% of the time and the Ga1B dimer is present 10.7% of the time. This results in a composition of $Ce_5Zn_{1.37}Ga_{17.73}$; crystallographic parameters are found in Table S3. This consistently observed defect may indicate that this structure is not particularly stable and may be kinetically trapped while transforming into $ThCr_2Si_2$-related structures.

$Ce_5Zn_{1.37}Ga_{17.73}$ reacts in the gallium flux below 750°C to form $CePdGa_6$-type compound $CeZn_{0.4}Ga_{6.6}$. This structure (Figure 9), like the Ce_2CuGa_{12} and Ce_2PdGa_{10} structures, can be viewed as an intergrowth of $ThCr_2Si_2$ slabs and MGa_2 antifluorite layers. It is assumed that the Zn occupies the 8-coordinate sites in the center of the Ga cubes in the antifluorite layers, which is occupied by Pd in the parent compound. Elemental analysis indicates a lower Zn content, so zinc and gallium are likely mixing in this site; their occupancy was fixed accordingly.

Magnetic Behavior. In all of these Ce/*T*/Ga compounds, the cerium ions form a square grid in the *ab*-plane and may exhibit either +3 or +4 valence, which will be reflected in the magnetic properties. The late transition metals are not likely to have a magnetic moment since their *d*-orbital derived bands are filled and positioned below the Fermi level. Figures 11 and 12 show temperature-dependent magnetic susceptibility $\chi(T)$ data obtained for the $ThCr_2Si_2$-type $CePd_{0.32}Ga_{3.68}$ and $CeCu_{0.37}Ga_{3.63}$ single crystals, with the magnetic field of 500 Oe applied parallel and perpendicular to the crystallographic *ab*-plane. The temperature-dependent data for both compounds were fitted using the Curie–Weiss law $1/\chi_m = (T/C) - (\theta/C)$ at high temperature (in the paramagnetic state, 100 K $\leq T \leq$ 300 K). The magnetic moment per cerium ion for $CePd_{0.32}Ga_{3.68}$ calculated from the curie constant C is μ_{eff} = 2.69 μ_B, close to the expected value of 2.54 μ_B for trivalent cerium. The Weiss constant was found to be θ = 5.26 K, indicating the presence of weak ferromagnetic coupling forces. This is in agreement with the sharp rise in susceptibility that occurs at 5.5 K, indicating ferromagnetic ordering. The magnetic behavior is strongly anisotropic, with much higher susceptibility when collected with the applied field parallel to the *ab*-plane. This is supported by the magnetization data collected at 2 K which also shows higher magnetization in the *ab*-plane, indicating that the Ce^{3+} moments lie in this plane.

For $CeCu_{0.37}Ga_{3.63}$, the magnetic moment per cerium ion, μ_{eff} = 2.51 μ_B, also agrees with trivalent cerium. The Weiss constant was found to be θ = 20.12 K, indicating ferromagnetic coupling forces that induce the observed ordering at low temperatures shown by the sharp rise in susceptibility that occurs at 7.2 K. As is the case with the Pd analogue, the susceptibility is anisotropic, with the Ce^{3+} moments also lying in the *ab*-plane. Similar behavior was reported for $CeCu_xGa_{4-x}$ compounds by Kontani and Pikul.[24,25] The magnetization data collected at 2 K are more complex for the Cu analogue,

https://doi.org/10.1021/acs.inorgchem.4c00797
Inorg. Chem. XXXX, XXX, XXX−XXX

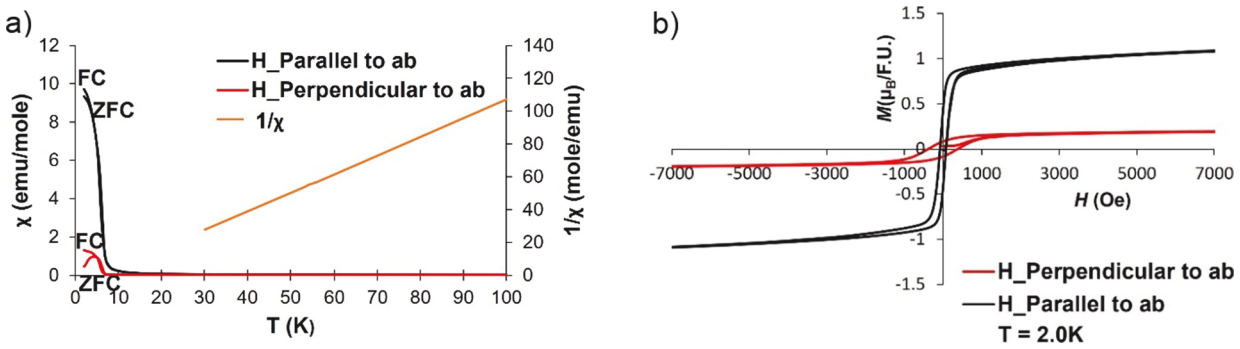

Figure 14. Magnetic susceptibility data for $Ce_5Zn_{1.37}Ga_{17.73}$. (a) Temperature-dependent magnetic susceptibility (χ) and inverse magnetic susceptibility ($1/\chi$) data; ZFC (zero-field cooled) and FC (field-cooled) splitting for both parallel (black) and perpendicular (red) orientations of the *ab*-plane to the applied field of H = 500 Oe. (b) Field dependence of magnetization collected at 2 K in both orientations.

showing soft ferromagnetic behavior with slightly higher remnant magnetization and coercive fields and a spin reorientation at 500 Oe. The saturation behavior is very similar to that of the Pd analogue, with an M_{sat} of 1.25 μ_B/fu and an M_{sat} of 0.25 μ_B/fu parallel and perpendicular to the *ab*-plane, respectively. The hysteresis loop in parallel orientation yields the remnant magnetization (M_R) of 0.75 μ_B per formula unit with a low coercive field, where the perpendicular orientation shows a higher coercive field (H_C) of around 1000 Oe with a remnant magnetization (M_R) of approximately 0.19 μ_B per formula unit. This group's previous work on isostructural $CeNi_{0.74}Ga_{3.26}$ similarly showed a strongly anisotropic soft ferromagnet; the Ce^{3+} moments ordered at 5.5 K aligned in the *ab*-plane, resulting in an M_{sat} of 1.3 μ_B/fu.[11]

Data for the high-temperature products $Ce_5T_xGa_{19-x}$ with the Rb_5Hg_{19} structure type are shown in Figures 13 and 14. For $Ce_5Ag_{1.76}Ga_{17.29}$, the data in Figure 13 indicate a magnetic moment per cerium ion, μ_{eff} = 2.38 μ_B which is close to the predicted value of 2.54 μ_B for trivalent cerium. The Weiss constant was found to be θ = 19.14 K, indicating ferromagnetic coupling forces which induce the observed ordering at low temperature shown by the sharp rise in susceptibility that occurs at 5.3K. As is the case with the CeT_xGa_{4-x} compounds, the susceptibility is anisotropic, with the Ce^{3+} moments also lying in the *ab*-plane. The magnetization data collected at 2 K shows soft ferromagnetic behavior with an M_{sat} of 1.00 μ_B/fu and an M_{sat} of 0.25 μ_B/fu parallel and perpendicular to the *ab*-plane, respectively. The hysteresis loop in parallel orientation yields the remnant magnetization (M_R) of 0.62 μ_B per formula unit with low coercive field, where the perpendicular orientation shows a higher coercive field (H_C) of around 500 Oe with a remnant magnetization (M_R) of approximately 0.20 μ_B per formula unit.

Fitting the data in Figure 14 indicates that the magnetic moment per cerium ion for the $Ce_5Zn_{1.37}Ga_{17.73}$ analogue is μ_{eff} = 2.68 μ_B, which is in close proximity with the expected value of 2.54 μ_B for trivalent cerium. The measured Weiss constant, θ = 4.91 K, suggests that there are weak ferromagnetic coupling forces that cause the observed ordering at low temperatures, as evidenced by the steep increase in susceptibility at 7.5 K. The susceptibility is again strongly anisotropic, with the Ce^{3+} moments also lying in the *ab*-plane. The Zn analogue's magnetization data, which was obtained at 2 K, exhibited soft ferromagnetic behavior. The saturation behavior is very similar to that of the Ag analogue, with an M_{sat} of 1.00 μ_B/fu and an M_{sat} of 0.20 μ_B/fu parallel and perpendicular to the *ab*-plane, respectively. The perpendicular orientation exhibits a greater coercive field (H_C) of around 500 Oe with a remnant magnetization (M_R) of roughly 0.10 μ_B per formula unit, while the parallel orientation of the hysteresis loop provides a remnant magnetization (M_R) of 0.50 μ_B per formula unit with low coercive field.

CONCLUSIONS

For the reactions of cerium with late transition metals (T = Cu, Zn, Pd, Ag) studied here, it was consistently observed that reactions quenched at high temperatures yielded different products than those of the same reaction quenched at low temperatures. All of the compounds exhibit tetragonal structures that are related to the $ThCr_2Si_2$ structure type, with layers of cerium (in square nets in the *ab*-plane) encapsulated by cages of gallium and transition metal atoms. It is noteworthy that the high-temperature products react as the system is cooled to generate compounds that incorporate more gallium in slabs intergrown with the $ThCr_2Si_2$-type layers (Figure S6). While the exact temperature of the transition is not known, the information did enable the isolation of crystals of the high-temperature compounds $CeCu_{0.37}Ga_{3.63}$, $CePd_{0.32}Ga_{3.68}$, $Ce_5Zn_{1.37}Ga_{17.73}$, and $Ce_5Ag_{1.76}Ga_{17.29}$. All of these are soft ferromagnets, with Ce^{3+} moments aligning in the *ab*-plane below 10 K. It is notable that their corresponding low-temperature phases are all reported to exhibit antiferromagnetic ordering.[18,19,22] The addition of gallium slabs to the structure serves to space the cerium square nets further apart along the *c*-axis, which modifies the magnetic coupling that occurs. Further investigation of Ce/T/Ga systems is needed to explore the effects of variation in elemental ratios and quenching temperatures, as well as the temperature dependence of systems with different transition metal elements such as T = Fe, Co, Ru, or Au.

ASSOCIATED CONTENT

Supporting Information

The Supporting Information is available free of charge at https://pubs.acs.org/doi/10.1021/acs.inorgchem.4c00797.

Product compositions; additional crystallographic data; SEM-EDS spectra; magnetic susceptibility data; and images of structures observed in this work (PDF)

Accession Codes

CCDC 2324748−2324751 contain the supplementary crystallographic data for this paper. These data can be obtained free of charge via www.ccdc.cam.ac.uk/data_request/cif, or by

https://doi.org/10.1021/acs.inorgchem.4c00797
Inorg. Chem. XXXX, XXX, XXX−XXX

emailing data_request@ccdc.cam.ac.uk, or by contacting The Cambridge Crystallographic Data Centre, 12 Union Road, Cambridge CB2 1EZ, UK; fax: +44 1223 336033.

AUTHOR INFORMATION

Corresponding Author

Susan E. Latturner − *Department of Chemistry, Florida State University, Tallahassee, Florida 32306, United States;* orcid.org/0000-0002-6146-5333; Email: slatturner@fsu.edu

Authors

Md. Sahab Uddin − *Department of Chemistry, Florida State University, Tallahassee, Florida 32306, United States*

Amirhossein Zareihassangheshlaghi − *Department of Chemistry, Florida State University, Tallahassee, Florida 32306, United States*

Complete contact information is available at: https://pubs.acs.org/10.1021/acs.inorgchem.4c00797

Notes

The authors declare no competing financial interest.

ACKNOWLEDGMENTS

This research was supported by the Division of Materials Research of the National Science Foundation (DMR-2126077). This investigation made use of the FSU X-ray Characterization Center (FSU075000XRAY), which is part of the Department of Chemistry and Biochemistry; we thank Dr. Xinsong Lin for his assistance with this equipment. We also made use of the scanning electron microscopy apparatus housed in the Florida State University's Department of Biology's Biological Sciences Imaging Resource (BSIR); we appreciate Dr. Eric Lochner for his assistance with this instrument.

REFERENCES

(1) Kalychak, Y. M.; Zaremba, V. I.; Baranyak, V. M.; Bruskov, V. A.; Zavalii, P.Yu Crystalline Structures of Compounds RCoIn5 (R = Ce, Pr, Nd, Sm, Gd, Tb, Dy, Ho, Y) and R2 CoIn8 (R = Ce, Pr, Nd, Sm, Gd, Dy, Ho, Er, Tm, Y). *Russ. Metall.* **1989**, *1*, 213−215.

(2) Chan, J. Y.; Olmstead, M. M.; Kauzlarich, S. M.; Webb, D. J. Structure and Ferromagnetism of the Rare-Earth Zintl Compounds: $Yb_{14}MnSb_{11}$ and $Yb_{14}MnBi_{11}$. *Chem. Mater.* **1998**, *10* (11), 3583−3588.

(3) Wolfers, P.; Obbade, S.; Fruchart, D.; Verhoef, R. Precise Crystal and Magnetic Structure Determinations. Part I: A Neutron Diffraction Study of Nd2Fe14B at 20 K. *J. Alloys Compd.* **1996**, *242* (1−2), 74−79.

(4) Richter, D.; Hempelmann, R.; Vinhas, L. A. Hydrogen Diffusion in LaNi5H6 Studied by Quasi-Elastic Neutron Scattering. *J. Common Met.* **1982**, *88* (2), 353−360.

(5) Latturner, S. E. Clusters, Assemble: Growth of Intermetallic Compounds from Metal Flux Reactions. *Acc. Chem. Res.* **2018**, *51* (1), 40−48.

(6) Kanatzidis, M. G.; Pöttgen, R.; Jeitschko, W. The Metal Flux: A Preparative Tool for the Exploration of Intermetallic Compounds. *Angew. Chem., Int. Ed.* **2005**, *44* (43), 6996−7023.

(7) Adriano, C.; Mendonça-Ferreira, L.; Bittar, E. M.; Pagliuso, P. G. Crystal Structure and Low Temperature Physical Properties of Ho2CoGa8 Intermetallic Antiferromagnet. *J. Appl. Phys.* **2008**, *103* (7), 07B712.

(8) Francisco, M. C.; Malliakas, C. D.; Macaluso, R. T.; Prestigiacomo, J.; Haldolaarachchige, N.; Adams, P. W.; Young, D. P.; Jia, Y.; Claus, H.; Gray, K. E.; Kanatzidis, M. G. Structures and Phase Transitions of CePd3+xGa8-x: New Variants of the BaHg11 Structure Type. *J. Am. Chem. Soc.* **2012**, *134* (31), 12998−13009.

(9) Latturner, S. E.; Bryan, J. D.; Blake, N.; Metiu, H.; Stucky, G. D. Siting of Antimony Dopants and Gallium in Ba8Ga16Ge30 Clathrates Grown from Gallium Flux. *Inorg. Chem.* **2002**, *41* (15), 3956−3961.

(10) Goforth, A. M.; Hope, H.; Condron, C. L.; Kauzlarich, S. M.; Jensen, N.; Klavins, P.; MaQuilon, S.; Fisk, Z. Magnetism and Negative Magnetoresistance of Two Magnetically Ordering, Rare-Earth-Containing Zintl Phases with a New Structure Type: EuGa2Pn2 (Pn = P, As). *Chem. Mater.* **2009**, *21* (19), 4480−4489.

(11) Haddock, J. W.; Barton, Z. J.; Feng, K.; Baumbach, R. E.; Zhang, Q.; Latturner, S. E. Flux Growth of Cerium Nickel Gallides Studied by In Situ Neutron Diffraction. *Inorg. Chem.* **2022**, *61* (39), 15645−15653.

(12) Vasquez, G.; Huq, A.; Latturner, S. E. In Situ Neutron Diffraction Studies of the Metal Flux Growth of Ba/Yb/Mg/Si Intermetallics. *Inorg. Chem.* **2019**, *58* (12), 8111−8119.

(13) *CrysAlisPRO; Oxford Diffraction*; Agilent Technologies UK Ltd.: Yarnton, England, 2023.

(14) Sheldrick, G. M. Crystal Structure Refinement with *SHELXL*. *Acta Crystallogr. Sect. C Struct. Chem.* **2015**, *71* (1), 3−8.

(15) Menard, M. C.; Drake, B. L.; McCandless, G. T.; Thomas, K. R.; Hembree, R. D.; Haldolaarachchige, N.; DiTusa, J. F.; Young, D. P.; Chan, J. Y. A Tale of Two Polymorphs − Growth and Characterization of α-$LnNiGa_4$ (Ln = Y, Gd−Yb) and β-$LnNi_{1-x}Ga_4$ (Ln = Tb−Er). *Eur. J. Inorg. Chem.* **2011**, *2011* (26), 3909−3919.

(16) Peng, L.; Chen, E.; Liu, S.; Liu, X.; Yu, Y. *In Situ* High-Temperature Nuclear Magnetic Resonance Characterization of Structural Evolution in Pure Gallium Melt. *Phys. Rev. B* **2019**, *100* (10), No. 104113.

(17) Xiong, L. H.; Wang, X. D.; Yu, Q.; Zhang, H.; Zhang, F.; Sun, Y.; Cao, Q. P.; Xie, H. L.; Xiao, T. Q.; Zhang, D. X.; Wang, C. Z.; Ho, K. M.; Ren, Y.; Jiang, J. Z. Temperature-Dependent Structure Evolution in Liquid Gallium. *Acta Mater.* **2017**, *128*, 304−312.

(18) Macaluso, R. T.; Millican, J. N.; Nakatsuji, S.; Lee, H.-O.; Carter, B.; Moreno, N. O.; Fisk, Z.; Chan, J. Y. A Comparison of the Structure and Localized Magnetism in Ce2PdGa12 with the Heavy Fermion CePdGa6. *J. Solid State Chem.* **2005**, *178* (11), 3547−3553.

(19) Menard, M. C.; Xiong, Y.; Karki, A. B.; Drake, B. L.; Adams, P. W.; Fronczek, F. R.; Young, D. P.; Chan, J. Y. Crystal Growth and Properties of Ln2Ag1−xGa10−y (Ln = La, Ce), a Disordered Variant of the Ce2NiGa10-Structure Type. *J. Solid State Chem.* **2010**, *183* (9), 1935−1942.

(20) Grin, Yu. N.; Hiebl, K.; Rogl, P.; Noël, H. Magnetism and Structural Chemistry of Ternary Gallides RENixGa4−x(RE ≡; La, Ce, Pr, Nd, Sm, Gd, Tb) and LaCo0.5Ga3.5. *J. Common Met* **1990**, *162* (2), 361−369.

(21) Grin, Yu. N.; Hiebl, K.; Rogl, P. Valence Behavior of Cerium in Ternary Gallides. *J. Common Met.* **1985**, *110* (1), 299−305.

(22) Cho, J. Y.; Millican, J. N.; Capan, C.; Sokolov, D. A.; Moldovan, M.; Karki, A. B.; Young, D. P.; Aronson, M. C.; Chan, J. Y. Crystal Growth, Structure, and Physical Properties of Ln_2MGa_{12} (*Ln* = La, Ce; *M* = Ni, Cu). *Chem. Mater.* **2008**, *20* (19), 6116−6123.

(23) Verbovytskyy, Y.; Gonçalves, A. P. The $BaAl_4$ Structure and Its Derivatives from the R-Zn-Ga Systems. *Solid State Phenom.* **2012**, *194*, 5−9.

(24) Kontani, M.; Motoyama, G.; Nishioka, T.; Murase, K. Magnetic properties of $CeCu_xAl_{4-x}$ and $CeCu_xGa_{4-x}$ single crystals. *Physica B* **1999**, *259*−*261*, 24−25.

(25) Przybylski, P.; Pikul, A. P.; Kaczorowski, D.; Wisniewski, P. Magnetic and related properties of the solid solution $CeCu_xGa_{4-x}$. *J. Phys. Chem. Solids* **2014**, *75*, 1284−1288.

https://doi.org/10.1021/acs.inorgchem.4c00797
Inorg. Chem. XXXX, XXX, XXX−XXX